J. Fluid Mech. (2013), *vol.* 720, *pp.* 338–356.
doi:10.1017/jfm.2013.14

Flow domain identification from free surface velocity in thin inertial films

C. Heining[1,†], T. Pollak[1] and M. Sellier[2]

[1]Applied Mechanics and Fluid Dynamics, University of Bayreuth, Universitätsstraße, 95440 Bayreuth, Germany

[2]Department of Mechanical Engineering, University of Canterbury, Private Bag 4800, Christchurch 8140, New Zealand

(Received 12 September 2011; revised 12 October 2012; accepted 2 January 2013; first published online 27 February 2013)

We consider the flow of a viscous liquid along an unknown topography. A new strategy is presented to reconstruct the topography and the free surface shape from one component of the free surface velocity only. In contrast to the classical approach in inverse problems based on optimization theory we derive an ordinary differential equation which can be solved directly to obtain the inverse solution. This is achieved by averaging the Navier–Stokes equation and coupling the function parameterizing the flow domain with the free surface velocity. Even though we consider nonlinear systems including inertia and surface tension, the inverse problem can be solved analytically with a Fourier series approach. We test our method on a variety of benchmark problems and show that the analytical solution can be applied to reconstruct the flow domain from noisy input data. It is also demonstrated that the asymptotic approach agrees very well with numerical results of the Navier–Stokes equation. The results are finally confirmed with an experimental study where we measure the free surface velocity for the film flow over a trench and compare the reconstructed topography with the measured one.

Key words: flow control, interfacial flows (free surface), thin films

1. Introduction

The gravity-driven flow of a viscous liquid along curved or uneven substrates occurs in many industrial and environmental systems. In industry, these kinds of flows can be found in coating applications (Kistler & Schweizer 1997; Weinstein & Ruschak 2004), heat and mass exchangers (Webb 1994; Kanaris & Mouza 2006), and many others. For such small-scale flows, capillary and wetting phenomena tend to prevail and we refer to the review of Craster & Matar (2009) for an exhaustive treatment of the underpinning mathematical models. In nature, gravity-driven film flows occur at a larger scale and typically capillary and wetting phenomena are of secondary importance. These flows are encountered in debris, glacier and lava flows, and in avalanches (Hutter, Svendsen & Rickenmann 1994), to name a few examples. Irrespective of the length scale, for Newtonian liquids, small Reynolds numbers and flat inclines the film flow is steady and establishes a parabolic velocity profile

† Email address for correspondence: tms@uni-bayreuth.de

(Spurk & Aksel 2008). If a critical Reynolds number is exceeded the free surface becomes unstable with respect to a long-wave instability. The stability and the transition to nonlinear, wavy regimes of the flow over a flat incline have been studied extensively over the last decades, for a review we refer to Chang (1994). If the incline is not flat but corrugated, undulated or modified with a topographic structure, the steady configuration already shows a rich variety of phenomena. These effects include the formation of hydraulic jumps (Wierschem & Aksel 2004), resonant states (Wierschem *et al.* 2008; Heining *et al.* 2009) and the formation and suppression of eddies (Wierschem *et al.* 2010). Furthermore, experimental results suggest that corrugated topographies can stabilize film flows (Vlachogiannis & Bontozoglou 2002; Wierschem, Lepski & Aksel 2005). This fact was confirmed numerically (Dávalos-Orozco 2007) and recently it has been shown that surface tension can lead to a destabilization of the system (D'Alessio, Pascal & Jasmine 2009; Häcker & Uecker 2009; Heining & Aksel 2010).

The numerous studies of the direct problem reveal that a topography can modify the free surface shape and the flow structure in film flows. A systematic control of the flow structure and the free surface shape leads to the corresponding inverse problem. Instead of prescribing a fixed topography, another quantity for example the free surface shape or the free surface velocity is prescribed but the topography and the flow field are unknown. First results on the inverse problem for film flows have been published by Sellier (2008), Sellier & Panda (2010) and Heining, Sellier & Aksel (2012) who derived the inverse solution in the lubrication approximation for creeping thin films. They studied the case where a target free-surface shape is achieved by modifying the topography shape. Instead of solving the inverse problem in the classical partial differential equation (PDE)-constrained optimization framework the lubrication approximation is rearranged, leading to a direct solution. The same approach was generalized by Heining & Aksel (2009) who considered inertial effects for the inverse problem by studying a weighted-residual integral boundary-layer model (Oron & Heining 2008). They also found that a steady wavy free surface is more stable than the corresponding flat one. Gessese *et al.* (2011) and Gessese & Sellier (2012) applied a similar method to reconstruct the river bed topography from free surface data within the shallow-water framework. Furthermore, Heining (2011) proposed an iterative numerical scheme to solve the inverse problem for the full Navier–Stokes equation and a given free surface shape. We note that similar inverse problems were solved by Lonyangapuo *et al.* (1999, 2001) but for inviscid and irrotational flows.

The inverse problem in film flow has many applications in experimental systems. The first is to reconstruct the flow field and the topography from the knowledge of free surface data only. Applications can be found in coating systems, in sedimentation flows with opaque liquids where the flow field and the underlying topographic structures are unknown or in geophysical flows for example in glaciology where the unknown basal glacier velocity is reconstructed from known data on the surface of the glacier (Maxwell *et al.* 2008).

Most of the previous publications on the inverse problem in film flow have in common that the flow field and the topography is reconstructed from the free surface shape only. In some applications, however, it is more convenient to prescribe or to measure the free surface velocity. Free surface velocity measurements can be implemented with an optical particle tracking which is less elaborate compared with measurements of the internal flow field. In some cases, for example for opaque liquids it is even impossible to determine the internal flow field by optical measurements.

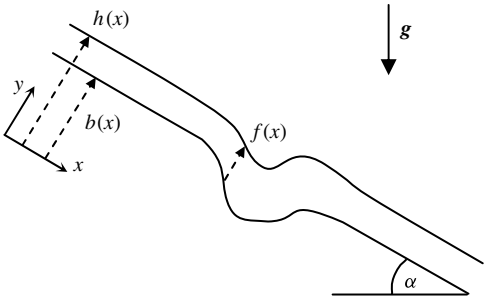

FIGURE 1. Viscous film flowing down an incline with inclination angle α. The substrate topography is $b(x)$, the free surface position $h(x)$ and the film thickness $f(x)$, respectively. The coordinate system is denoted by (x, y). The driving force is gravity $\boldsymbol{g}$.

The same applies for glacier flows where the bedrock can only be inferred by expensive radar measurements. The task is to reconstruct the flow domain and the flow field from the knowledge of the free surface velocity only. In the following, we derive a method which enables us to determine the flow domain including the free surface shape and bottom topography from the given free surface velocity data in thin films including inertia.

The outline of the article is as follows. First, we derive the governing equations for the direct and the inverse problem. While the direct problem is solved numerically, we find an analytical solution for the inverse problem. In § 3 the inverse solution is studied in detail. We use the data of the direct problem to validate the inverse solution procedure and to determine its sensitivity with respect to noisy input data. Furthermore, the inverse solution is validated with data from the Navier–Stokes equation. In addition, we perform a series of experiments to show how to reconstruct the topography in applications. Finally, in § 4 we summarize our results and discuss the main conclusions.

2. Mathematical formulation

2.1. *Governing equations*

The steady gravity-driven motion of a fluid with density ρ and kinematic viscosity ν is governed by the Navier–Stokes equation and the continuity equation

$$(\boldsymbol{u}\cdot\nabla)\boldsymbol{u} = -\frac{1}{\rho}\nabla p + \boldsymbol{g} + \nu\nabla^2\boldsymbol{u}, \quad \nabla\cdot\boldsymbol{u} = 0, \tag{2.1}$$

where $\boldsymbol{u} = (u, v)$ is the velocity vector, p the pressure, $\boldsymbol{g} = g(\sin\alpha, -\cos\alpha)$ the gravity vector, g the gravitational constant and α the inclination angle. An overview of the system is depicted in figure 1. At the solid wall $y = b$ the fluid satisfies the no-slip and the no-penetration boundary condition $\boldsymbol{u} = \boldsymbol{0}$. At the free surface, located at $y = h$, we have the kinematic boundary condition

$$v = uh_x, \tag{2.2}$$

where the subscript denotes differentiation with respect to the corresponding variable. The dynamic boundary condition at the free surface reads in tensor notation

$$\boldsymbol{n}\cdot\boldsymbol{T} = -\sigma\kappa\boldsymbol{n}, \tag{2.3}$$

where $\boldsymbol{n}$, $\boldsymbol{T}$, κ and σ are the unit outer normal vector of the free surface, the stress tensor, the curvature of the free surface and surface tension, respectively. The components of (2.3) read, after some algebraic manipulations and neglecting the viscosity of the overlying air,

$$2h_x(v_y - u_x) + (1 - h_x^2)(u_y + v_x) = 0. \tag{2.4}$$

$$\eta[h_x(u_y + v_x) - 2v_y] + p - p_0 + \sigma \frac{h_{xx}}{(1 + h_x^2)^{3/2}} = 0, \tag{2.5}$$

where p_0 denotes the pressure at the free surface and η the dynamic viscosity.

Since the flow is unperturbed far away from the topographical feature we can assume that the flow is given there by the Nusselt velocity profile with

$$u_N(y) = \frac{gd^2 \sin\alpha}{2\nu} \left[1 - \left(1 - \frac{y}{d}\right)^2\right], \tag{2.6}$$

where d is the constant Nusselt film thickness which can be adjusted by changing the flow rate q in the system. In (2.6) the (x, y) coordinate system is located at the flat substrate. Applying the integral mass conservation to (2.6) yields a relation between the flow rate and the Nusselt film thickness:

$$q = \int_0^d u_N \, \mathrm{d}y = \frac{d^3 g \sin\alpha}{3\nu}. \tag{2.7}$$

In the following, we use the quantities of the Nusselt flow as a reference and scale the velocities and lengths accordingly. We take the mean velocity $\bar{u} = q/d$ of the corresponding Nusselt flow as the characteristic scale of the velocity in the x-direction. The Nusselt film thickness d serves as the characteristic length scale in the y-direction while the x-direction is scaled with the channel length L. Summarizing, the scaling reads

$$b = db^*, \quad f = df^*, \quad h = dh^* \tag{2.8a}$$

$$x = Lx^*, \quad y = dy^*, \quad u = \bar{u}u^* \tag{2.8b}$$

$$v = \varepsilon\bar{u}v^*, \quad p = \rho\bar{u}^2 p^* \tag{2.8c}$$

where variables with stars indicate dimensionless quantities. We furthermore introduced the dimensionless film thickness parameter $\varepsilon = d/L$ characterizing the ratio of the vertical length scale compared with the horizontal length scale. It has to be noted that ε could also be interpreted as a dimensionless slope, see Aksel (2000). Substituting the scaling (2.8) into the field equations and the boundary conditions and omitting the superscript, we obtain for the two components of the Navier–Stokes equation and the continuity equation:

$$\varepsilon Re(uu_x + vu_y) = -\varepsilon Rep_x + 3 + \varepsilon^2 u_{xx} + u_{yy}, \tag{2.9a}$$

$$\varepsilon^2 Re(uv_x + vv_y) = -Rep_y - 3\cot\alpha + \varepsilon^3 v_{xx} + \varepsilon v_{yy}, \tag{2.9b}$$

$$u_x + v_y = 0, \tag{2.9c}$$

where we introduced the Reynolds number $Re = \bar{u}d/\nu$. At the substrate $y = b$ the no-slip and no-penetration condition yield $u = v = 0$. The kinematic boundary condition at $y = h$ is given by $v = uh_x$ and the two components of the dynamic boundary condition read

$$2\varepsilon^2 h_x(v_y - u_x) + (1 - \varepsilon^2 h_x^2)(u_y + \varepsilon^2 v_x) = 0, \tag{2.10}$$

$$Rep - Rep_0 + \varepsilon h_x(u_y + \varepsilon^2 v_x) - 2\varepsilon v_y + 3Bo^{-1}\frac{h_{xx}}{(1+\varepsilon^2 h_x^2)^{3/2}} = 0, \tag{2.11}$$

where we defined the inverse Bond number $Bo^{-1} = \sigma/(L^2\rho g \sin\alpha)$, a dimensionless measure for surface tension relative to gravity.

2.2. *Thin-film approximation*

The previous scaling and modelling is valid for general films. In the following, we simplify the analysis by considering films where the length scale in the y-direction is small compared with that in the x-direction which is equivalent to the assumption that the dimensionless film thickness parameter ε is small. In order to take into account inertia, surface tension and the hydrostatic pressure, we assume that $\varepsilon Re = O(1)$, $\varepsilon Bo^{-1} = O(1)$, $\varepsilon\cot\alpha = O(1)$, and truncate terms of the order ε^2 and higher. This allows us to study inertial regimes with Reynolds numbers up to $Re = O(100)$ as long as the flow is steady and stable.

After applying the thin film approximation the field equations read

$$\varepsilon Re(uu_x + vu_y) = -\varepsilon Rep_x + 3 + u_{yy}, \tag{2.12a}$$

$$0 = -Rep_y - 3\cot\alpha. \tag{2.12b}$$

The continuity equation, the no-slip and no-penetration condition at the wall, and the kinematic boundary condition remain unchanged. For the two components of the dynamic boundary condition at the free surface $y = h$, we obtain

$$u_y = 0, \tag{2.13}$$

$$Rep - Rep_0 + 3Bo^{-1}h_{xx} = 0. \tag{2.14}$$

After integrating the second equation in (2.12) and substituting (2.14) we can solve for the pressure

$$Rep = 3\cot\alpha(h - y) + Rep_0 - 3Bo^{-1}h_{xx}. \tag{2.15}$$

Inserting this expression into the Navier–Stokes equation in the x-direction, we obtain

$$\varepsilon Re(uu_x + vu_y) = -3\varepsilon\cot\alpha h_x + 3\varepsilon Bo^{-1}h_{xxx} + 3 + u_{yy}. \tag{2.16}$$

The dynamic boundary condition (2.14) and pressure have been eliminated.

Integrating the continuity equation from the topography $y = b$ to the free surface $y = h$ and substituting the kinematic boundary condition yields an integral expression of the continuity equation:

$$q_x = 0, \tag{2.17}$$

where we defined the flow rate in a cross-section in the x-direction

$$q = \int_b^h u\,\mathrm{d}y. \tag{2.18}$$

To obtain an integral expression for the Navier–Stokes equation we integrate (2.16) from the substrate to the free surface which yields

$$\varepsilon Re\left(\frac{\mathrm{d}}{\mathrm{d}x}\int_b^h u^2\,\mathrm{d}y\right) = (-3\varepsilon\cot\alpha h_x + 3\varepsilon Bo^{-1}h_{xxx})f + 3f - u_y|_{y=b}, \tag{2.19}$$

where we made use of the continuity equation to eliminate the velocity component v and the dynamic boundary conditions (2.13).

The averaged Navier–Stokes equation (2.19) and the integral continuity equation (2.17) depend on the velocity u, the film thickness f and the free surface position h. We note that the film thickness is related to the free surface position by $f = h - b$. In order to close the system a specific velocity profile has to be imposed in the following.

2.3. *Integral boundary-layer model for the direct problem*

In the case of the steady, unidirectional flow over a flat incline the parabolic velocity profile is an exact analytical solution of the Navier–Stokes equation. For the two-dimensional flow along a wavy wall, experiments by Wierschem, Scholle & Aksel (2002) show that a parabolic velocity profile is an accurate approximation if the bottom steepness is moderate. From the theoretical point of view it can be shown that for the flow along a moderate topography the leading-order solution is governed by a parabolic velocity profile (see Dávalos-Orozco 2007). Accordingly, we assume that the velocity profile $u(x, y)$ is coupled with the free surface position by a self-similar parabolic profile of the form

$$u = \frac{3}{f}\left[\frac{y-b}{f} - \frac{1}{2}\left(\frac{y-b}{f}\right)^2\right]. \tag{2.20}$$

The velocity profile (2.20) fulfils: (i) the no-slip condition at the substrate; and (ii) the remaining component of the dynamic boundary condition (2.13). Furthermore, we find that (2.20) conserves the mass which can easily be confirmed by (2.17). Substituting (2.20) into the integral momentum balance yields (see also Trifonov 1998)

$$\varepsilon Re\frac{6}{5}\frac{\mathrm{d}}{\mathrm{d}x}\left(\frac{1}{f}\right) = \left[-3\varepsilon\cot\alpha\,(b+f)_x + 3\varepsilon Bo^{-1}\,(b+f)_{xxx}\right]f + 3f - \frac{3}{f^2}, \tag{2.21}$$

which is a nonlinear ordinary differential equation for the film thickness $f(x)$. For a given topography function $b(x)$, equation (2.21) can be solved numerically, assuming periodic boundary conditions.

2.4. *Integral boundary-layer model for the inverse problem*

The velocity profile for the direct problem (2.20) is coupled with the film thickness only. In the following we reparameterize $u(x, y)$ and write the velocity profile as a function of the film thickness and the free surface velocity.

We assume that the velocity fulfils

$$u = 2u_S\left[\frac{y-b}{f} - \frac{1}{2}\left(\frac{y-b}{f}\right)^2\right], \tag{2.22}$$

where $u_S(x)$ is the free surface velocity. It has to be noted that the v-component can be obtained by integrating the continuity equation but is not needed for the further calculations. The form of (2.22) is chosen such that: (i) the no-slip condition at the substrate; and (ii) the remaining component of the dynamic boundary condition (2.13) are fulfilled. Choosing a parabolic velocity profile is furthermore motivated by three observations: (i) the flow field far away from the topography is parabolic; (ii) the leading-order velocity profile in the lubrication limit is parabolic. Häcker & Uecker (2009) have shown that this is also valid in the presence of inertia as long as the topography modulation is moderate; (iii) for the same problem Wierschem *et al.* (2005) demonstrated by a series of experiments that the velocity profile is

locally parabolic. Also, Veremieiev *et al.* (2010) performed an exhaustive comparative study of the error induced in a depth-averaged formulation based on a parabolic velocity profile, analogous to that used here, relative to full Navier–Stokes solutions for thin film flows over steps up or down. As expected, this error is largest for larger Reynolds numbers and higher topographies (relative to the undisturbed film thickness). The maximum reported error between the depth-averaged formulation and the full Navier–Stokes solution is around 5.5 % for a step-up and 12 % for a step-down for a Reynolds number of the order of 30 and a step height as high as the asymptotic film thickness. On that basis, we hence expect reasonable results, as long as the depth and the curvature of the topography are moderate.

Substituting (2.22) into (2.19) yields

$$\varepsilon Re \frac{\mathrm{d}}{\mathrm{d}x}\left(\frac{8}{15}u_S^2 f\right) = \left(-3\varepsilon \cot\alpha h_x + 3\varepsilon Bo^{-1} h_{xxx}\right) f + 3f - \frac{2u_S}{f}, \tag{2.23}$$

which is the integral momentum balance written in terms of u_S. Substituting (2.22) into (2.18) we find that $q = (2/3)u_S f$. After integrating the mass balance (2.17) and setting the integration constant to one we can relate the film thickness with the free surface velocity

$$f = \frac{3}{2u_S}. \tag{2.24}$$

We note that a similar expression was found by Aksel (2000) for the creeping film flow down an inclined plane with an edge. The dependence $u_S \sim 1/f$ is not obvious at first glance since the dimensional velocity field (2.6) yields the relation $u_S \sim d^3$. However, the mass conservation proposes a constant volume flux which has the consequence that a smaller film thickness implies a larger free surface velocity, see (2.24).

We can now eliminate the film thickness from (2.23) and obtain

$$-3\varepsilon \cot\alpha h_x + 3\varepsilon Bo^{-1} h_{xxx} = \frac{2}{3}\left[\frac{2}{5}\varepsilon Re \frac{\mathrm{d}}{\mathrm{d}x}(u_S^2) - \frac{9}{2} + \frac{4u_S^3}{3}\right], \tag{2.25}$$

which is an inhomogeneous linear ordinary differential equation with constant coefficients for the free surface shape h with the inhomogeneous forcing coming from the free surface velocity. Equation (2.25) is complemented by periodic boundary conditions. Equation (2.21) and (2.25) will be referred to as integral boundary-layer model (IBL) for the direct and the inverse problem, respectively.

Solving (2.25) enables us to determine the position of the free surface with the knowledge of the free surface velocity u_S. Once the free surface position is solved the topography shape can be determined by $b = h - f$ where the film thickness f is given by (2.24). It is worth mentioning that only the component of the free surface velocity in the mean plane of motion is necessary to reconstruct the flow domain. Furthermore, we note that for applications with noisy input data (2.25) can be integrated once to eliminate the derivative of u_S^2. Compared with previous approaches (Sellier 2008; Heining & Aksel 2009; Sellier & Panda 2010; Heining 2011), the present method can be formulated without higher derivatives of the input data. This is an immense advantage since the input data contains possible noise which is amplified by taking the derivative up to the third-order (see Heining & Aksel 2009).

In the following, we solve (2.25) by a Fourier series approach. The right-hand side of (2.25) is represented as a Fourier series $\sum_{k=-N}^{N} r_k \mathrm{e}^{\mathrm{i}kx}$ where the coefficients r_k

are determined with a standard fast Fourier routine. We also represent the free surface position as a Fourier series $h = \sum_{k=-N}^{N} h_k e^{ikx}$ with unknown coefficients h_k. Equation (2.25) then reduces to a set of $2N + 1$ algebraic equations of the form $r_k = [-3\varepsilon \cot\alpha (ik) + 3\varepsilon Bo^{-1} (ik)^3] h_k$, $k = -N, \ldots, N$ which has the simple solution

$$h_k = r_k \left[-3\varepsilon \cot\alpha ik + 3\varepsilon Bo^{-1} (ik)^3\right]^{-1} \quad \text{for } k \in \{-N, \ldots, N\}/\{0\}. \tag{2.26}$$

The zeroth Fourier coefficient h_0 corresponds to a constant offset and is yet undetermined but can be chosen arbitrarily. We remark that the solution (2.26) depends on ε, $\cot\alpha$, Bo^{-1}; the influence of inertia is implicitly included in the Fourier coefficients r_k.

3. Solution of the inverse problem

3.1. *Comparison of the inverse solution to the direct solution*

To test our method we solve the inverse problem for free surface data which is already known from the direct problem. We obtain the free surface velocity profiles by first solving the direct problem (2.21) for a given topography and subsequently solving the inverse problem for the free surface velocity determined by evaluating (2.20) at $y = h$.

As a first test case we consider the flow over a trench topography given by the non-dimensional expression

$$b = \frac{\xi}{2}\left\{\tanh\left(\frac{x - x_2}{\delta}\right) - \tanh\left(\frac{x - x_1}{\delta}\right)\right\} \tag{3.1}$$

where δ (typical value 0.001) is a measure for the smoothness of the edges, x_1, x_2 the coordinates of the edges of the trench and $\xi = a/d$ its non-dimensional height. We choose the geometry parameters $L = 0.1$ m, $a = 5 \times 10^{-3}$ m, trench width 0.01 m, inclination angle $\alpha = 8°$ and fluid parameters $\nu = 1.158 \times 10^{-5}$ m^2 s^{-1}, $\rho = 924$ kg m^{-3} and $\sigma = 18.9 \times 10^{-3}$ N m^{-1}. We note that the fluid corresponds to a silicone oil which was also used in the experimental study by Wierschem *et al.* (2010). For $Re = 10$ this yields the dimensionless parameters $\varepsilon = 0.0143$, $\cot\alpha = 7.1154$, $Bo^{-1} = 0.001499$ and $\xi = 3.4876$. The trench has a dimensionless width of 0.1. For this configuration we first solve the direct problem by solving the integral boundary-layer model (2.21) numerically with a finite-difference scheme and periodic boundary conditions. After solving for the film thickness we can determine the velocity field which is coupled with the film thickness, according to (2.20). It is then possible to compute the free surface velocity by $u_S = 3/(2f)$. From this expression we note that the system has a singularity if the film thickness tends to zero which is a consequence of mass conservation (Aksel 2000). However, this case is excluded since the film thickness is assumed to have non-negative values ($f > 0$) everywhere, assuming fully wetting conditions.

The numerical results of the direct problem are shown in figure 2. We find that the free surface shows a ridge before entering in the trough. This was already pointed out in previous theoretical (Kalliadasis, Bielarz & Homsy 2000) and experimental studies (Decré & Baret 2004). In addition, the free surface velocity increases considerably at the inflow into the trough, compare also with Aksel (2000). In what follows we take the free surface velocity data of the direct problem, see figure 2, as input data for the inverse problem. In other words we determine the topography and the free surface shape for the given free surface velocity. The solution of the direct problem is a benchmark for the inverse problem which allows us to test the method. In the ideal case both solutions should exactly coincide if the accuracy is sufficient.

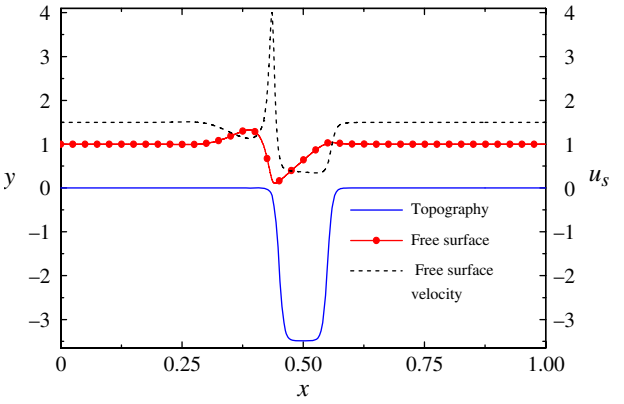

FIGURE 2. (Colour online) Numerical solution of the direct problem (2.21). The parameters are given in the text.

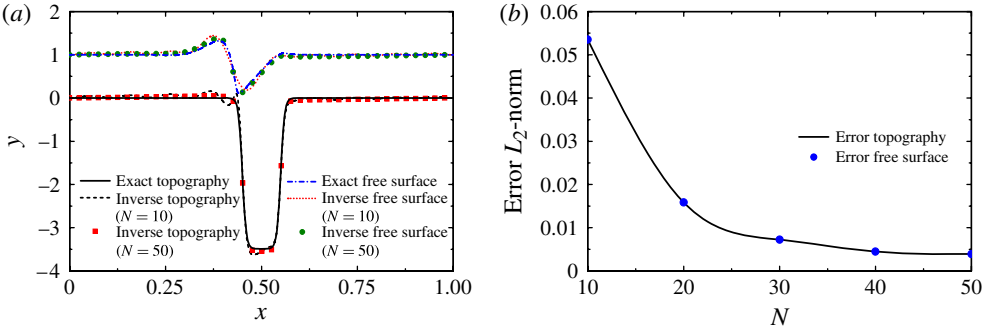

FIGURE 3. (Colour online) (*a*) The reconstruction of the free surface profile and the topography shape for the free surface velocity given in figure 2. (*b*) The L_2-norm of the error for increasing number of Fourier modes.

We compute the Fourier decomposition of the right-hand side of (2.25) with the Matlab fft routine. Subsequently, the series solution (2.26) is evaluated for different values of N. In figure 3(*a*) we show the inverse solution for $N = 10$ and $N = 50$. We find that even though the free surface velocity has steep gradients which could produce oscillations in a Fourier analysis, the original topography and free surface shape is already predicted accurately for $N = 10$. For $N = 50$ the direct solution and the reconstructed solution show a perfect agreement with no visible deviation. To visualize the influence of the number of Fourier modes on the reconstruction we plot in figure 3(*b*) the L_2-norm of the error of the free surface shape and the topography for increasing N. As expected the error decreases and takes for example the value 0.0039 for $N = 50$.

Finally, we compare the results of the present analysis which includes the influence of inertia to previous studies in the low-Reynolds-number limit based on the lubrication approximation. For the following example we fix the dimensionless parameters $\delta = 0.01$, $Bo^{-1} = 0.001$, $\cot\alpha = 3$, $\xi = 0.2$ and change the Reynolds number from $Re = 5$ to $Re = 20$ to focus on the influence of inertia. The results

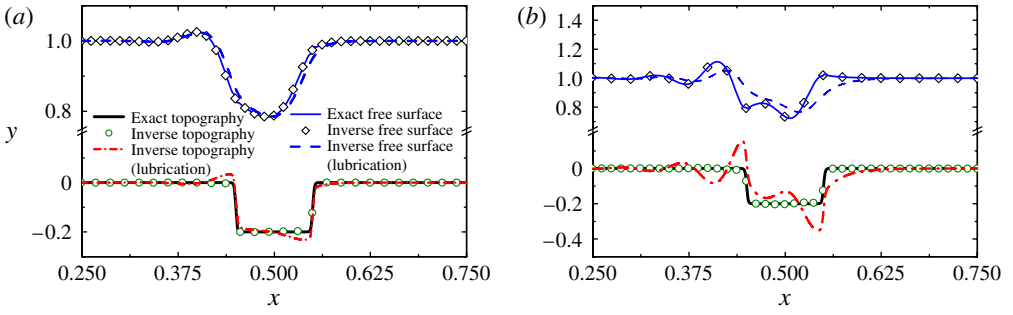

FIGURE 4. (Colour online) (*a*,*b*) Comparison of the lubrication approximation and the present approach for $Re = 5$ and $Re = 20$. The solid lines represent the exact topography and free surface shape, circles and diamonds the inverse solution with the present analytical approach and dashed and dashed dotted lines show the inverse solution based on the lubrication approximation. For the sake of clarity we only show data close to the trench.

are shown in figure 4 where we compare the results of the lubrication approximation which is valid for $Re = O(1)$ with the present approach with the validity up to $\delta Re = O(1)$. As can be seen in figure 4(*a*) the results agree well for $Re = 5$. For the example in figure 4(*b*) the lubrication approximation is not valid and yields results which are not useable compared to the results of the analytical solution including the influence of inertia.

3.2. *Sensitivity with respect to noisy input data*

In real systems, however, for example in applications where the free surface velocity is measured experimentally, the input data for the inverse problem is not smooth but contains measurement inaccuracies. We test such a case by superimposing artificial noise to the free surface velocity in figure 2. Therefore, we define the new free surface velocity $\tilde{u}_s = u_s + \tilde{\varepsilon}\mu(x)$ where $\tilde{\varepsilon}$ is the magnitude of the disturbance and $\mu(x)$ is a random variable distributed uniformly between -0.5 and 0.5 which leads to a maximum deviation between u_S and $\tilde{u}_s$ of $\max(\tilde{u}_s/u_S) = 1 + 0.5\tilde{\varepsilon}/\min(u_S)$. Figure 5 shows two examples for $\tilde{\varepsilon} = 0.1$ and $\tilde{\varepsilon} = 0.5$ with maximum deviation between u_S and $\tilde{u}_s$ of 14.4 and 72.2 %.

We find that in both cases, figure 5(*a*,*b*), the free surface shape can be reconstructed with more success than the topography shape. The reason for the good agreement lies in the Fourier approach. Since the Fourier series is truncated at a finite wavenumber we simultaneously truncate higher frequencies which is equivalent to a filtering of the noisy input signal. The asymptotic approach automatically leads to a smoothing of the solution. The inverse solution is hence robust with respect to high-frequency disturbances of the input data. This is a major benefit since many inverse problems are ill-posed in the sense that the solution does not depend continuously on the input data with the consequence that small changes in the input data create significant changes in the solution (Engl, Hanke & Neubauer 2000). In many cases this requires explicit regularization techniques.

3.3. *Reconstruction of the flow domain from data obtained by the Navier–Stokes equation*

The previous results present the reconstruction of the flow geometry from free surface data achieved by the integral boundary-layer model. Now, we verify our approach by comparing the results to numerical calculations of the full Navier–Stokes equation.

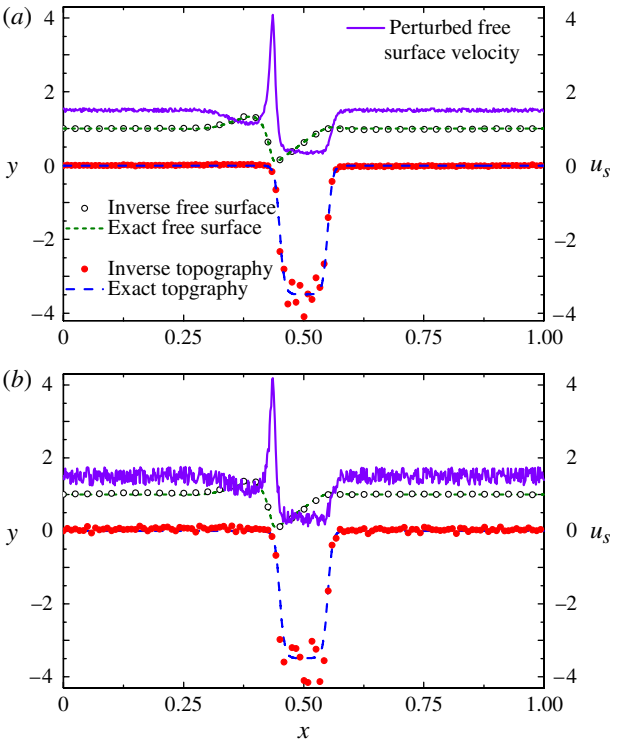

FIGURE 5. (Colour online) Reconstruction of the free surface profile and the topography shape for the disturbed free surface velocity $\tilde{u}_s = u_s + \tilde{\varepsilon}\mu(x)$ for $N = 60$: (*a*) $\tilde{\varepsilon} = 0.1$; (*b*) $\tilde{\varepsilon} = 0.5$.

In the following, the free surface velocity u_S comes from numerical results of the Navier–Stokes equation throughout the whole section. The data for the direct problem is taken from the literature and the study is completed with our own numerical computations. To begin with, we consider the film flow of a viscous liquid along a wavy incline (Wierschem *et al.* 2010). Wierschem *et al.* (2010) investigated the corresponding direct problem. We now take that free surface velocity calculated by a finite element analysis of the Navier–Stokes equation to determine the corresponding free surface and topography shape by the present asymptotic solution of the inverse problem. The solution is shown in figure 6.

It is found that the reconstructed free surface shape is in good agreement with the original free surface data from the Navier–Stokes equation. The reconstructed bottom shows a deviation in the form of a phase shift with respect to the original data; however, the qualitative agreement is still acceptable.

The results in figure 6 suggest that the analytical reconstruction based on the free surface velocity from the Navier–Stokes equation is possible for smoothly varying topographies. In the following we pick up the examples from the beginning and study again a trench topography. There are several publications considering the flow over a trench experimentally (e.g. Decré & Baret 2004) and numerically (e.g. Kalliadasis *et al.* 2000). However, none of these publications study the free surface velocity which is necessary to reconstruct the topography with the present method. As a way out, we now solve the Navier–Stokes equation numerically and determine the

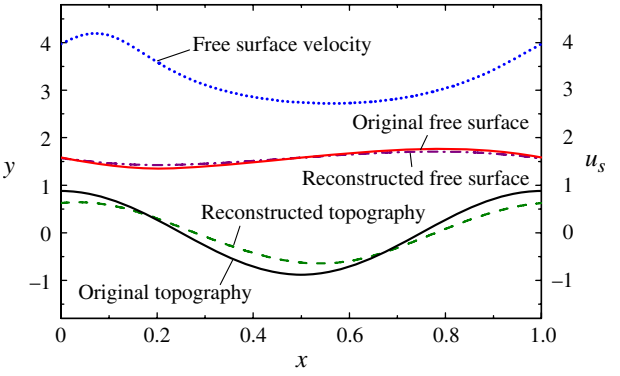

FIGURE 6. (Colour online) Solution of the inverse problem for the data in Wierschem *et al.* (2010). The dimensionless parameters are $Re = 5$, $\cot\alpha = 7.1154$, $Bo^{-1} = 0.15$ and $\varepsilon = 0.1138$. The dimensionless amplitude of the topography is 0.8788. The free surface velocity is shifted upwards by two for the sake of clarity.

free surface velocity. We consider water as a working liquid with kinematic viscosity $\nu = 1\times10^{-6}\text{m}^2\ \text{s}^{-1}$, density $\rho = 1000\ \text{kg m}^{-3}$ and surface tension $\sigma = 72\times10^{-3}\ \text{N m}^{-1}$. The inclination angle is chosen as $\alpha = 5.05°$, the trench width is 6 mm and the length of the domain is $L = 12$ mm. The Reynolds number is set to $Re = 10$ which yields a Nusselt film thickness $d = 0.326$ mm. The depth of the trench is set to 0.326 mm. This leads to the following dimensionless parameters: $Bo^{-1} = 0.5864$, $\cot\alpha = 11.3163$, $\varepsilon = 0.0272$ and $\xi = 1$.

We solve the Navier–Stokes equation numerically with the VOF method implemented in the OpenFOAM package. Details can be found in Pak & Hu (2011) and the references therein. The results of the direct problem are shown in figure 7(*a*). We observe that the free surface is smoothly undulated and the flow field shows a separation behind the step down. It has to be noted that recirculation cannot be captured by the integral boundary-layer model because the specific choice of the velocity profile (see (2.20) and (2.22)) does not take flow reversal into account. For the reconstruction of the flow domain in figure 7(*a*) it is necessary to determine the free surface velocity. The results are given in figure 7(*b*), where we compare the free surface velocity of the numerical results of the Navier–Stokes equation (VOF) with the numerical results of the direct integral boundary-layer equation (2.21). Except for the steep gradients both results show a good qualitative agreement. It is intuitively clear that the quality of the inverse reconstruction depends on the agreement of the direct VOF and the direct IBL solution. The better the direct IBL solution approximates the VOF solution the better the flow geometry is reconstructed in the inverse problem. From the shapes of the free surface velocity obtained by the VOF and the IBL in figure 7(*b*) we conclude that the reconstruction might be inaccurate at the sides of the topography. Figure 7(*c*) shows the original data of the VOF method together with the analytical reconstruction with $N = 15$ modes. It is found that the shape of the reconstructed free surface agrees well with the original one; increasing the number of modes does not yield an improvement. The topography is reconstructed at the flat parts but shows deviations at the step-down and the step up. The reconstructed topography is much smoother than the rectangular original. Nevertheless, the reconstruction predicts well the depth of the trench even though the

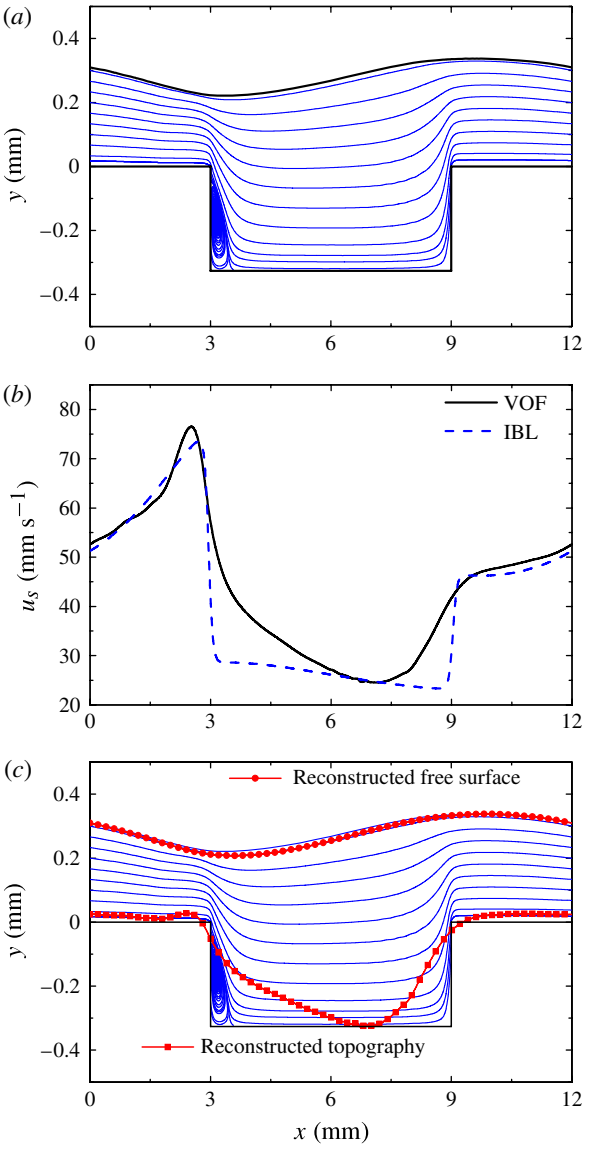

FIGURE 7. (Colour online) (*a*) The solution of the direct problem. The solid lines indicate the free surface, the streamlines and the topography. (*b*) The free surface velocities from the VOF method and from the IBL-equation. (*c*) The solution of the direct problem (solid lines), the reconstructed free surface (line with circles) and the reconstructed topography (line with boxes). The inverse solution is obtained for $N = 15$.

flow field shows a recirculation which is strictly speaking beyond the applicability of the IBL model. Even though our theory does not account for flow reversal and the parameters in this example are out of the domain of validity we find a reasonable agreement in the free surface shape.

In figure 7 the depth of the trench has the same magnitude as the Nusselt film thickness. In the following, we decrease the depth of the trench and study the

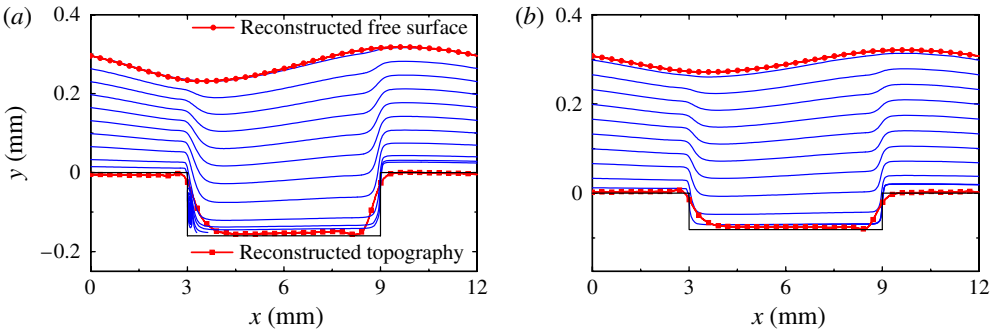

FIGURE 8. (Colour online) Reconstruction of the topography and the free surface shape for trenches with depth $d/2$ (a) and $d/4$ (b), the other dimensionless parameters are identical to figure 7. The inverse solution is obtained for $N = 15$. Lines indicate the streamlines of the VOF solution while the inverse free surface and topography is labelled with dots and boxes, respectively.

behaviour of the inverse solution while the other parameters are kept constant. In figure 8(a) the trench has a depth of $d/2$ and only a very small flow separation can be observed after the step down. As in the previous example the free surface is reconstructed successfully, while the reconstructed topography matches the flat parts but shows some deviations near the sharp edges. Similar results are obtained for the reconstruction of the flow over a trench with height $d/4$, see figure 8(b). The inverse solution recovers again the free surface shape but smoothes the edges of the topography. We remark that increasing the number of modes does not improve the solution significantly. Summarizing, we can derive an *a posteriori* estimate of the quality of the reconstruction. Since the parabolic velocity profile is only valid for smooth topographies with $\xi \ll 1$ we can estimate whether the reconstruction is reasonable. After solving the inverse problem, an inverse steepness parameter is determined by taking $\xi_i =$ (amplitude of topography)/(film thickness). The smaller the parameter is, the better the reconstruction. This can also be observed in figures 7 and 8 where the inverse steepness parameter is gradually reduced from $\xi_i \approx 1$ to $\xi_i \approx 0.25$. In all cases, the free surface shape is well reconstructed which is an important new result in itself.

3.4. *Reconstruction of experimental data*

To verify the applicability of our proposed method we carry out experiments and compare the reconstruction of the topography with the actual measured geometry. The experiments have been carried out in a channel of 170 mm width which is inclined by an angle of $\alpha = 9.7 \pm 0.05^\circ$ with respect to the horizontal. The underlying topography is of the trench type used in §§ 3.2 and 3.3, see also (3.1), with a depth of $a = 0.96 \pm 0.01$ mm and a length of $L = 30.04 \pm 0.01$ mm. An eccentric pump type *AFJ 15.2 B* from Jöhstadt provides an adjustable volume flux q from a large liquid reservoir into a smaller inflow tank on top of the channel. Driven by gravity the liquid flows from the small inflow tank down the channel through the test section as illustrated in figure 9(a).

The thickness of the corresponding Nusselt film is measured with an accuracy of 5 μm with a micrometre screw far downstream of the trench feature in a flat region of the channel. The liquid properties density, kinematic viscosity and surface tension

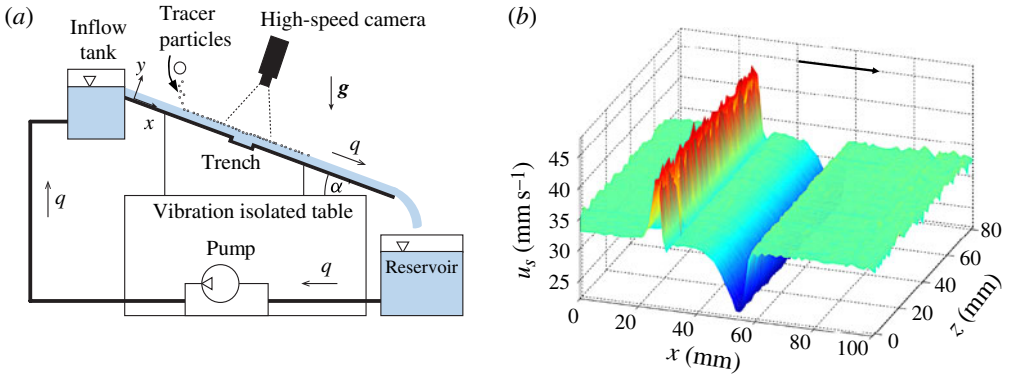

FIGURE 9. (Colour online) (*a*) Experimental setup. (*b*) The free surface velocity distribution $u_s(x, y)$ over a 80 mm broad patch. The flow direction is from left to right.

d (mm)	T (° C)	ρ (g cm^{-3})	η (mPa s)	σ (mN m^{-1})
1.480	23.7	0.9512	50.97	19.80
1.745	23.7	0.9512	50.97	19.80
2.025	23.9	0.9511	53.36	19.78

TABLE 1. Physical properties of the silicone oil and Nusselt film thickness of the three experimental runs.

of the silicone oil we used as a test liquid are given in table 1. Furthermore, table 1 shows the Nusselt film thickness of the three experiments. During each experimental run the temperature of the liquid was constant within 0.1 °C.

The free surface velocity of the liquid is measured in a patch of approximately 100 mm in downstream (x-) direction and approximately 80 mm in crosswise (z-) direction, including the topography feature, in the middle of the channel, using a monochrome CCD high-speed camera which is installed above the channel. As tracer particles we use an active carbon powder which is strewed on the free surface of the liquid far upstream of the recorded patch. Owing to surface tension the vast majority of these particles remain at the free surface of the liquid and float passively with the liquid without sinking into the bulk fluid. Images of the particles are captured at 125 or 250 fps at the camera's full resolution of 1280 × 1024 pixels. The projection of the velocity field into the (x, z)-plane can be computed from these images using a particle tracking algorithm based on *polyparticletracker* (Rogers *et al.* 2007). After the evaluation of at least 1000 frames per experimental run we could interpolate the velocity field. A typical result of the interpolated free surface velocity is plotted in figure 9(*b*). We also refer to Heining, Pollak & Aksel (2012) who applied a similar experimental technique to measure the two-dimensional velocity field. In the present case, it is not the whole two-dimensional velocity field $u_s(x, z)$ that is required but only the component in the downstream direction. Since the particle tracking yields the velocity field in many cross-sections we can use the averaging to enhance the velocity field's quality and to remove noise.

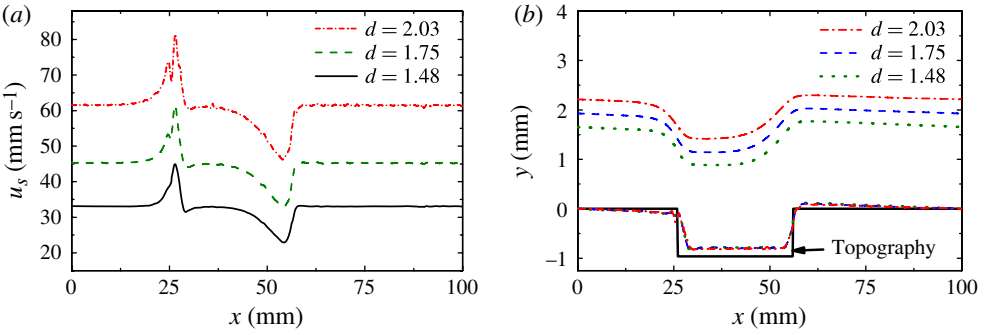

FIGURE 10. (Colour online) (*a*) The experimental free surface velocity for three different flow rates. In (*b*) we take this velocity as input to reconstruct the topography and the corresponding free surface shape. The inverse topography for all three film thicknesses does not show any distinguishable difference.

After averaging we obtain a smooth velocity component in the x-direction which, for the three Nusselt film thicknesses, is shown in figure 10(*a*). The Reynolds number for the three experiments is $Re = 0.58, 0.94, 1.48$. For a flow along a flat incline these values guarantee stable flow, however, inertia is of the order of $O(1)$ and not negligible. We now apply the analytical reconstruction technique to this velocity to reconstruct the flow domain. The results of the analysis is shown in figure 10(*b*). Similar to the reconstruction of the Navier–Stokes data in § 3.3 the reconstruction of the flat parts of the topography shows a good agreement. For all three Nusselt film thicknesses, the topography has an identical shape. Only the sharp corners of the topography and the level of the trench show some deviations from the actual trench.

In addition to the results in § 3.2 where we demonstrated that the inverse solution is robust with respect to high-frequency disturbances we show that the method is robust with respect to other, non-statistical error sources, as they also occur in experiments. To summarize, we show that our analytical solution enables us to reconstruct the flow domain. Even for opaque liquids where information about the topography is covered by the liquid we can determine the flow geometry only by measurements of the free surface velocity.

4. Discussion and conclusion

A method has been derived to reconstruct the flow domain from a known free surface velocity in thin inertial gravity-driven film flow. It is shown that only one velocity component is sufficient to solve the inverse problem. Instead of solving the inverse problem in the conventional optimization framework, we derive a model which couples the flow domain, namely the free surface and bottom shape, with one component of the free surface velocity. This is achieved by averaging the Navier–Stokes equation over the flow domain and introducing a specific velocity profile. As a consequence the inverse problem can be solved with similar methods compared with the direct problem. Although the direct problem is nonlinear and has to be solved numerically we find analytical solutions of the inverse problem. By assuming periodic boundary conditions a Fourier series approach is applied to determine the flow domain. Compared with previous inverse approaches the present

method can be written without higher derivatives of the input data which makes the inverse problem robust with respect to noisy input data.

The inverse problem is tested with solutions of the corresponding direct problem. First, we prescribe a topography, solve the direct problem and determine the free surface velocity. Subsequently, the inverse problem is solved analytically for this given free surface velocity. Adding artificial noise to the free surface velocity shows that the inverse problem is robust with respect to statistical errors. The reason therefore lies in the analytical solution which is represented as a truncated Fourier series. High-frequency noise is smoothed by truncating the Fourier series.

Furthermore, we show that the flow reconstruction based on one component of the free surface velocity agrees well with data from the Navier–Stokes equation. We therefore consider a case in the literature where the direct problem is studied for a wavy topography. We take the given free surface velocity to reconstruct the flow domain. It is shown that both the free surface and the topography can be reconstructed using the simple analytical Fourier series approach.

We also demonstrate that the reconstruction yields reasonable results for flows with flow recirculations and sharp topographies. The flow field and the free surface velocity are obtained with a VOF method for the full Navier–Stokes equation. We choose a case where the flow separates and establishes an eddy in the trench. Subsequently, the original free surface shape and the topography is reconstructed based on the analytical solution of the IBL equation. It is found that the free surface shape is successfully recovered while the topography is smoothed out but the qualitative agreement is still acceptable. A study on the trench depth reveals that the agreement between the numerical simulation of the direct problem and the analytical approximation of the inverse problem increases with decreasing trench depth. Deviations can be found only near sharp edges.

The validity of the reconstruction is finally underpinned with an experimental study. With an optical particle tracking method we are able to find the projected free surface velocity of the flow over a trench geometry. Since the experimental free surface velocity and the measurements are two-dimensional we can average the data to obtain a smooth velocity profile. After reconstructing the topography for different flow rates we find that, similar to the previous numerical results, the computed and the actual topography show a good agreement. This proves that the algorithm yields an effective tool to reconstruct the flow domain in typical applications where only the free surface velocity is accessible or available.

Acknowledgements

We acknowledge the support of Professor N. Aksel with valuable discussions and by giving us the possibility to use his laboratory and equipment for the experiments. The authors acknowledge the support of the BMBF project NZL 11/012 and of the New Zealand Royal Society, project FRG11-24.

REFERENCES

AKSEL, N. 2000 Influence of the capillarity on a creeping film flow down an inclined plane with an edge. *Arch. Appl. Mech.* **70**, 81–90.

ARGYRIAD, K., VLACHOGIANNIS, M. & BONTOZOGLOU, V. 2006 Experimental study of inclined film flow along periodic corrugations: the effect of wall steepness. *Phys. Fluids* **18**, 012102.

CHANG, H.-C. 1994 Wave evolution on a falling film. *Annu. Rev. Fluid Mech.* **26**, 103–136.

CRASTER, R. V. & MATAR, O. K. 2009 Dynamics and stability of thin liquid films. *Rev. Mod. Phys.* **81**, 1131–1198.

D'ALESSIO, S. J. D., PASCAL, J. P. & JASMINE, H. A. 2009 Instability in gravity-driven flow over uneven surfaces. *Phys. Fluids* **21**, 062105.

DÁVALOS-OROZCO, L. A. 2007 Nonlinear instability of a thin film flowing down a smoothly deformed surface. *Phys. Fluids* **19**, 074103.

DECRÉ, M & BARET, J. C. 2004 Gravity-driven flows of viscous liquids over two-dimensional topographies. *J. Fluid Mech.* **487**, 147–166.

ENGL, H. W., HANKE, M. & NEUBAUER, A. 2000 *Regularization of Inverse Problems*. Kluwer.

GESSESE, A. & SELLIER, M. 2012 A direct solution approach to the inverse shallow-water problem. *Math. Problems Engng* **2012**, 417950.

GESSESE, A. F., SELLIER, M., VANHOUTEN, E. & SMART, G. 2011 Reconstruction of river bed topography from free surface data using direct numerical approach in one-dimensional shallow water flow. *Inverse Problems* **27**, 025001.

HÄCKER, T. & UECKER, H. 2009 An integral boundary layer equation for film flow over inclined wavy bottoms. *Phys. Fluids* **21**, 092105.

HEINING, C. 2011 Velocity field reconstruction in gravity-driven flow over unknown topography. *Phys. Fluids* **23**, 032101.

HEINING, C. & AKSEL, N. 2009 Bottom reconstruction in thin-film flow over topography: steady solution and linear stability. *Phys. Fluids* **21**, 083605.

HEINING, C. & AKSEL, N. 2010 Effects of inertia and surface tension on a power-law fluid flowing down a wavy incline. *Intl J. Multiphase Flow* **36**, 847–857.

HEINING, C., BONTOZOGLOU, V., AKSEL, N. & WIERSCHEM, A. 2009 Nonlinear resonance in viscous films on inclined wavy planes. *Intl J. Multiphase Flow* **35**, 78–90.

HEINING, C., POLLAK, T. & AKSEL, N. 2012 Pattern formation and mixing in three-dimensional film flow. *Phys. Fluids* **24**, 042102.

HEINING, C., SELLIER, M. & AKSEL, N. 2012 The inverse problem in creeping film flows. *Acta Mechanica* **223**, 841–847.

HUTTER, K., SVENDSEN, B. & RICKENMANN, D. 1994 Debris flow modelling: a review. *Cont. Mech. Thermodyn.* **8**, 1.

KALLIADASIS, S., BIELARZ, C. & HOMSY, G. M. 2000 Steady free-surface thin film flows over topography. *Phys. Fluids* **12**, 1889–1898.

KANARIS, A. G. & MOUZA, A. A. 2006 Flow and heat transfer prediction in a corrugated plate heat exchanger using a CFD code. *Chem. Engng Technol.* **29**, 923–930.

KISTLER, S. F. & SCHWEIZER, P. M. 1997 *Liquid Film Coating*. Chapman & Hall.

LONYANGAPUO, J. K., ELLIOTT, L., INGHAM, D. B. & WEN, X. 1999 Retrieval of the shape of the bottom surface of a channel when the free surface profile is given. *Engng Anal. Bound. Elem.* **23**, 457–470.

LONYANGAPUO, J. K., ELLIOTT, L., INGHAM, D. B. & WEN, X. 2001 Solving free surface fluid flow problems by the minimal kinetic energy functional. *Intl J. Numer. Meth. Fluids* **37**, 577–600.

LUCA, I., HUTTER, K., THAI, Y. C. & KUO, C. Y. 2009 A hierarchy of avalanche models on arbitrary topography. *Acta Mech.* **205**, 121.

MAXWELL, D., TRUFFER, M., AVDONIN, S. & STUEFER, M. 2008 An iterative scheme for determining glacier velocities and stresses. *J. Glaciol.* **54**, 888–898.

ORON, A. & HEINING, C. 2008 Weighted-residual integral boundary-layer model for the nonlinear dynamics of thin liquid films falling on an undulating vertical wall. *Phys. Fluids* **20**, 082102.

PAK, M. I. & HU, G. H. 2011 Numerical investigations on vortical structures of viscous film flows along periodic rectangular corrugations. *Intl J. Multiphase Flow* **37**, 369–379.

ROGERS, S. S., WAIGH, T. A., ZHAO, X. & LU, J. R. 2007 Precise particle tracking against a complicated background: polynomial fitting with Gaussian weight. *Phys. Biol.* **4**, 220.

SELLIER, M. 2008 Substrate design or reconstruction from free surface data for thin film flows. *Phys. Fluids* **20**, 062106.

SELLIER, M. & PANDA, S. 2010 Beating capillarity in thin film flows. *Int. J. Numer. Meth. Fluids* **63**, 431–448.

SPURK, J. H. & AKSEL, N. 2008 *Fluid Mechanics*, 2nd edn. Springer.

TRIFONOV, Y. Y. 1998 Viscous liquid film flows over a periodic surface. *Intl J. Multiphase Flow* **24**, 1139–1161.

TRIFONOV, Y. Y. 2007 Stability and nonlinear wavy regimes in downward film flows on a corrugated surface. *J. Appl. Mech. Tech. Phys.* **48**, 91–100.

TUFFER, M. 2004 The basal speed of valley glaciers: an inverse approach. *J. Glaciol.* **50**, 236–242.

VLACHOGIANNIS, M. & BONTOZOGLOU, V. 2002 Experiments on laminar film flow along a periodic wall. *J. Fluid Mech.* **457**, 133–156.

VEREMIEIEV, S., THOMPSON, H. M., LEE, Y.-C. & GASKELL, P. H. 2010 Inertial thin film flow on planar surfaces featuring topography. *Comp. & Fluids* **39**, 431–450.

WEBB, R. L. 1994 *Principles of Enhanced Heat Transfer*. John Wiley & Sons.

WEINSTEIN, S. J. & RUSCHAK, K. J. 2004 Coating flows. *Annu. Rev. Fluid Mech.* **36**, 29.

WIERSCHEM, A. & AKSEL, N. 2004 Hydraulic jumps and standing waves in gravity-driven flows of viscous liquids in wavy open channels. *Phys. Fluids* **16**, 3868–3877.

WIERSCHEM, A., BONTOZOGLOU, V., HEINING, C., UECKER, H. & AKSEL, N. 2008 Linear resonance in viscous films on inclined wavy planes. *Intl J. Multiphase Flow* **34**, 580–590.

WIERSCHEM, A., LEPSKI, C. & AKSEL, N. 2005 Effect of long undulated bottoms on thin gravity-driven films. *Acta Mech.* **179**, 41–66.

WIERSCHEM, A., POLLAK, T., HEINING, C. & AKSEL, N. 2010 Suppression of eddies in films over topography. *Phys. Fluids* **22**, 113603.

WIERSCHEM, A., SCHOLLE, M. & AKSEL, N. 2002 Comparison of different theoretical approaches to experiments on film flow down an inclined wavy channel. *Exp. Fluids* **33**, 429–442.